ADVANCED MATERIALS
www.advmat.de

Local Electronic Structure of Molecular Heterojunctions in a Single-Layer 2D Covalent Organic Framework

Trinity Joshi, Chen Chen, Huifang Li, Christian S. Diercks, Gaoqiang Wang, Peter J. Waller, Hong Li, Jean-Luc Bredas, Omar M. Yaghi,* and Michael F. Crommie**

The synthesis of a single-layer covalent organic framework (COF) with spatially modulated internal potentials provides new opportunities for manipulating the electronic structure of molecularly defined materials. Here, the fabrication and electronic characterization of COF-420: a single-layer porphyrin-based square-lattice COF containing a periodic array of oriented, type II electronic heterojunctions is reported. In contrast to previous donor–acceptor COFs, COF-420 is constructed from building blocks that yield identical cores upon reticulation, but that are bridged by electrically asymmetric linkers supporting oriented electronic dipoles. Scanning tunneling spectroscopy reveals staggered gap (type II) band alignment between adjacent molecular cores in COF-420, in agreement with first-principles calculations. Hirshfeld charge analysis indicates that dipole fields from oriented imine linkages within COF-420 are the main cause of the staggered electronic structure in this square grid of atomically–precise heterojunctions.

Covalent organic frameworks (COFs) are 2D or 3D crystalline structures constructed from organic molecular building blocks stitched together through strong covalent bonds.[1] Different electronic and chemical properties can be engineered into COF networks by modifying the molecular properties of the building-blocks.[2] Two-component COFs provide a high degree of electronic tunability since one molecular element can act as a "core" while the second acts as a "linker" between cores, and both can be precisely modified.[3] This approach, for example, has been used to create donor-acceptor COFs that are made by either directly fusing donor/acceptor molecules into core/linker arrangements or by introducing either donor or acceptor guests into the pores of COFs to yield ordered arrays of molecular charge-transfer pairs, with potential applications in optoelectronics and catalysis.[4] Such electrically modulated COFs, however, have up to now been fabricated using techniques that do not allow synthesis of a single-layer structure, and no local probe measurements have been performed to verify the effects of local charge-transfer. Here we report a new technique for fabricating COFs that exhibit internal electronic heterojunctions with staggered potential offsets. The core of the COF is tuned independently from charge-transfer elements that are placed between adjacent cores. This is accomplished through directed Schiff-base condensation reactions that allow oriented dipoles to be placed between core elements in an alternating arrangement, thus causing adjacent cores to experience a relative potential offset. The surface compatibility of this chemistry allows bottom-up fabrication of single-layer

T. Joshi, Dr. C. Chen, Dr. G. Wang, Prof. M. F. Crommie
Department of Physics
University of California – Berkeley
Berkeley, CA 94720, USA
E-mail: crommie@berkeley.edu
H. Li, Dr. H. Li, Prof. J.-L. Bredas
Laboratory for Computational and Theoretical Chemistry of Advanced Materials
Physical Science and Engineering Division
King Abdullah University of Science and Technology
Thuwal 23955-6900, Kingdom of Saudi Arabia
hong.li@chemistry.gatech.edu
C. S. Diercks, P. J. Waller, Prof. O. M. Yaghi
Department of Chemistry
Kavli Energy NanoScience Institute and Berkeley Global Science Institute
University of California – Berkeley
Berkeley, CA 94720, USA
E-mail: yaghi@berkeley.edu
The ORCID identification number(s) for the author(s) of this article can be found under https://doi.org/10.1002/adma.201805941.
C. S. Diercks, P. J. Waller, Prof. O. M. Yaghi
Materials Sciences Division
Lawrence Berkeley National Laboratory
Berkeley, CA 94720, USA
Dr. H. Li, Prof. J.-L. Bredas
School of Chemistry and Biochemistry & Center for Organic Photonics and Electronics
Georgia Institute of Technology
901 Atlantic Drive NW, Atlanta, GA 30332-0400, USA
Prof. M. F. Crommie
Materials Sciences Division
Lawrence Berkeley National Laboratory
Berkeley, CA 94720, USA
Prof. M. F. Crommie
Kavli Energy NanoScience Institute
University of California Berkeley
Lawrence Berkeley National Laboratory
Berkeley, CA 94720, USA

DOI: 10.1002/adma.201805941

 © 2018 WILEY-VCH Verlag GmbH & Co. KGaA, Weinheim

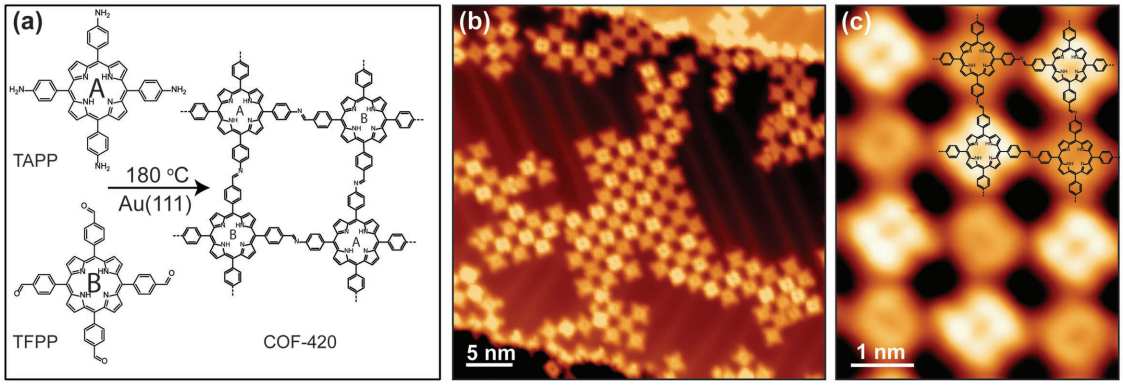

Figure 1. Bottom-up fabrication of COF-420. a) Schematic representation of the synthesis of COF-420 from molecular precursors TAPP and TFPP. b) Representative large-scale STM topographic image of COF-420 on Au(111) (sample bias V_s = 0.8 V, tunnel current I_t = 10 pA). c) Close-up STM image of COF-420 with the chemical structure overlaid in top-right corner (V_s = 0.8 V, I_t = 10 pA).

COF-420 whose local electronic structure we have characterized at the atomic scale using scanned probe microscopy.

The new COF was fabricated by first synthesizing two square planar tetratopic building blocks (5,10,15,20-tetrakis(4-aminophenyl)porphyrin (TAPP) and 5,10,15,20-tetrakis(4-formylphenyl)porphyrin (TFPP)) as shown in **Figure 1**. Upon reticulation at a surface these precursors yield cores that have identical chemical composition but are rendered electrically asymmetric by the relative orientation of the imine linkages connecting them. Charge-transfer functionality thus resides in the linker and is separated from the core electronic properties. This unique COF is termed COF-420 ([(TAPP)(TFPP)] imine) and exhibits a square lattice (**sql**) topology. Due to the asymmetrical configuration of the linkage (Figure 1a), each 5,10,15,20-tetraphenyl porphyrin core in COF-420 experiences a different chemical environment than its four nearest neighbor porphyrin cores. For example, if we denote cores arising from TAPP as "core A" and cores arising from TFPP as "core B", then the nitrogen atom of the imine linkage is the first atom encountered as one moves outward from core A, whereas for core B the first atom encountered is carbon. Scanning tunneling microscopy (STM) was used to experimentally verify that this asymmetrical bonding scheme results in the spatial separation of the conduction band (CB) and the valence band (VB) onto different porphyrin cores (i.e., different sublattices), thus forming a grid of molecular type II heterojunctions within COF-420. Hirshfeld charge analysis[5] performed using density functional theory (DFT) suggests that these molecular heterojunctions arise from dipole fields generated within the imine linkages of the COF.

The synthesis of single-layer COF-420 was carried out on a Au(111) surface in ultrahigh vacuum (UHV). TFPP molecules were first deposited onto the surface via thermal evaporation, followed by deposition of TAPP molecules (see Figure S6, Supporting Information for the electronic structure of the constituent molecules before reticulation into COF-420). The adsorbed precursors were then gradually annealed to 180 °C and held at that temperature for 45 min to induce the condensation reaction that results in imine bond formation (Figure 1a). Figure 1b shows an STM topographic image of the resulting single-layer COF-420. Square lattice patches are observed that exhibit a "checkerboard" pattern, indicating an alternating array of two electrically distinct porphyrin cores (a small fraction of cores near the edge of the COF do not exhibit the checkerboard pattern, possibly due to metalation of core B).[6] The unit cell determined via STM imaging has equal sides of length $a = b = 27 \pm 1.6$ Å. Figure 1c shows a zoomed-in image of COF-420, with a superimposed line drawing of the chemical structure in the top right corner. We are able to unambiguously identify the darker porphyrin cores as core A (originating from TAPP) and the brighter porphyrin cores as core B (originating from TFPP) through the use of subsidiary reaction with 2,5-dimethoxybenzene-1,4-dicarboxaldehyde (DMA) test molecules (see Section 3, Supporting Information, for details).

The local electronic structure of COF-420 was characterized by STM dI/dV point spectroscopy performed at different positions on the single-layer COF as shown in **Figure 2** (point spectroscopy positions are shown in Figure 2a). The black curve in Figure 2b shows a reference spectrum taken at a nearby bare Au(111) region (the sharp drop at –0.5 V corresponds to a Shockley surface state band edge[7]). The blue curve shows a typical dI/dV point spectrum recorded on core A within the COF, whereas the red curve shows a typical dI/dV point spectrum recorded on the neighboring core B. Both cores exhibit two well-defined resonances that arise from bands composed of porphyrin molecular orbitals. The bands localized on core A, however, are shifted up in energy by ≈0.25 eV relative to the bands whose weight lies on core B (i.e., the bands are localized on different sublattices). This causes the VB to lie on core A while the CB lies on core B. Similarly, the outlying VB–1 and CB+1 bands are located on core B and core A, respectively. The resulting experimental bandgap for COF-420 is 1.92 ± 0.06 eV (i.e., the difference in energy between the CB and VB peaks).

The spatial localization of the COF-420 bands onto different sublattices is better seen in the dI/dV maps of Figure 2c–f, obtained at the different peak energies in the same COF region as imaged in Figure 2a. Figure 2c shows the dI/dV map obtained at the CB energy, where the local density of states (LDOS) lights up (i.e., has highest intensity) on core B sites. The CB LDOS pattern at each core exhibits a nearly fourfold symmetric structure with two orthogonal nodal lines crossing through the center of the porphyrin core. The LDOS intensity at the VB energy is shown in Figure 2d, and is found to be shifted

© 2018 WILEY-VCH Verlag GmbH & Co. KGaA, Weinheim

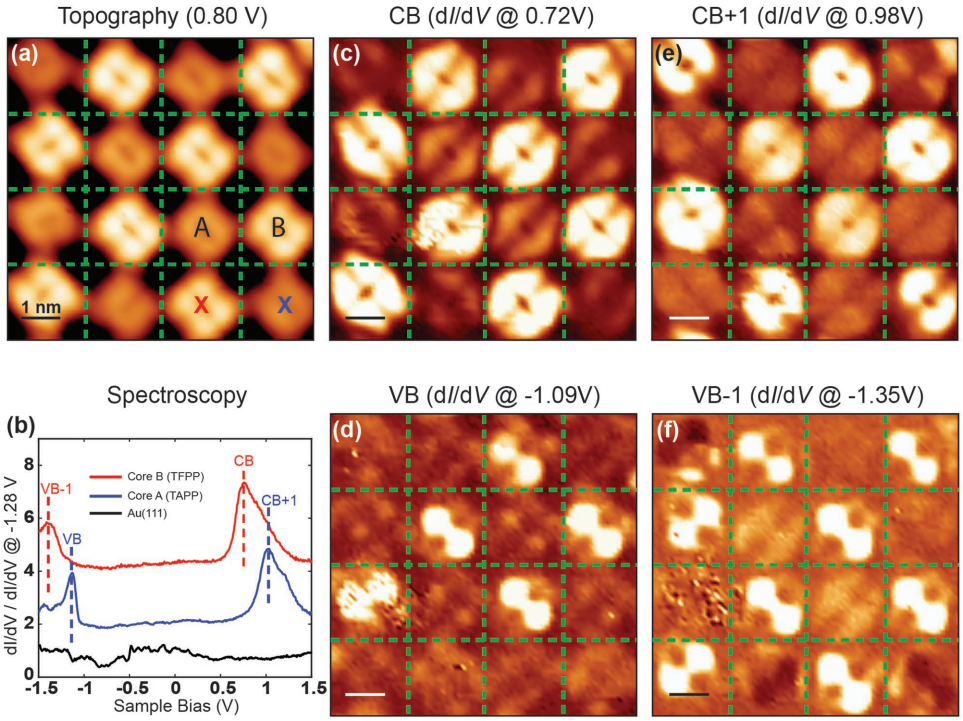

Figure 2. Electronic structure of COF-420. a) Close-up STM image of COF-420 (V_s = 0.8 V, I_t = 10 pA). Red and blue x's indicate the positions where dI/dV spectra were recorded. b) dI/dV spectra taken at location of core B (red curve) and core A (blue curve) shown in (a), as well as spectrum from bare Au(111) surface for reference (black curve). Each curve is normalized by the value at V_s = –1.28 V and the red (blue) curve is upshifted by 4 a.u. (1.75 a.u.) for clarity (open feedback set point parameters: V_s = 0.8 V, I_t = 20 pA for all the curves; modulation voltage V_{rms} = 10 mV). c–f) Experimental dI/dV maps for: c) the COF CB at 0.72 V, d) the COF VB at –1.09 V, e) the COF CB+1 at 0.98 V, and f) the COF VB–1 at –1.35 V (dI/dV map parameters: I_t = 20 pA; modulation voltage V_{rms} = 10 mV).

from core B sites to core A sites. The VB LDOS symmetry is also quite different than the CB LDOS in that it is "dumbbell" shaped and twofold symmetric rather than fourfold symmetric. The difference between the VB and CB LDOS shapes reflects the difference in symmetry between the highest occupied molecular orbital and the lowest unoccupied molecular orbital for isolated porphyrin molecules and their derivatives.[8] Unlike the CB states seen on the core B sublattice, some of the core A sites do not show LDOS intensity at the VB energy. This is caused by small, spatially inhomogeneous shifts in the energy of the VB peak, likely due to surface defects and conformational changes within the COF (including the number of complete nearest neighbor bonds). The VB peak has the narrowest width and so slight shifts in energy for molecules on the core A sublattice causes dramatic reductions in VB intensity in constant bias dI/dV maps. Figure 2e,f show that the CB+1 and VB-1 LDOS also reside separately at core A and core B sites, respectively, thus separating onto different sublattices just as seen for the VB and CB states. The COF-420 spectroscopy shows all of the hallmarks of type II heterojunctions, including a staggered band structure and spatial localization of VB and CB states at different physical locations. Unlike a conventional type II heterojunction which has only a single interface, COF-420 exhibits a periodic array of heterojunctions that exist between each adjacent molecular core.

In order to identify the underlying cause of the staggered band structure and wave function localization observed in our experiments, we performed first-principles calculations of COF-420 using DFT at the generalized gradient approximation (GGA) level. These efforts were aimed at answering three fundamental questions. The first question is simply whether DFT-based simulations are able to reproduce the experimental phenomena observed in order to confirm that it is consistent with the physical system we believe to be measuring. The second is whether this behavior is intrinsic to the COF, or rather a byproduct of the interaction between the COF and the Au(111) substrate. The third question is what microscopic mechanism causes type II heterojunction behavior to arise between the sublattices of COF-420.

We addressed the first question by modeling the behavior of COF-420 on Au(111) using the unit cell sketched in **Figure 3**a. The STM dI/dV spectra were simulated by separately calculating the projected density of states of this system onto core A and core B, as shown in Figure 3b. The core A sublattice (blue curve) shows two prominent peaks corresponding to the VB and CB+1 bands whereas core B (red curve) shows two peaks shifted down in energy with respect to core A (corresponding to the VB-1 and CB bands). The resulting bandgap is 1.10 eV, ≈0.82 eV smaller than the experimental value, which is due to the known behavior of GGA-DFT calculations to underestimate quasiparticle bandgaps.[9] Other than the gap, however, the calculation reproduces the experimental results closely. For example, the VB and CB are seen to localize on different sublattice cores, precisely as seen in the experiment (Figure S1, Supporting Information). Also, the energy differences between VB and VB-1 as well as between CB and CB+1 have an average

© 2018 WILEY-VCH Verlag GmbH & Co. KGaA, Weinheim

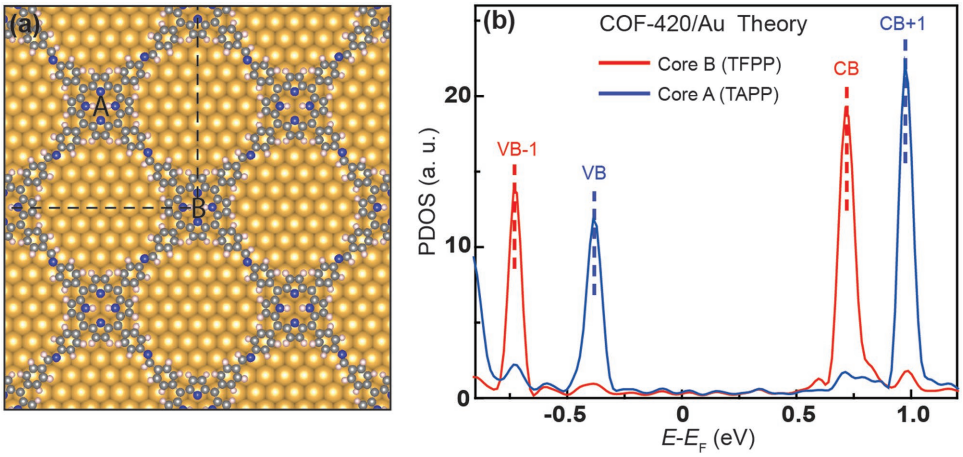

Figure 3. Theoretical electronic structure of COF-420. a) Optimized geometry of COF-420 on a Au(111) surface resulting from DFT calculation (unit cell marked by dashed lines). b) Theoretical PDOS calculated for COF-420 on Au(111) (i.e., DOS projected separately onto the two cores). The red curve represents the PDOS of core B whereas the blue curve represents the PDOS of core A.

magnitude of 0.31 eV, very close to the average experimental value of 0.25 eV (these differences do not suffer the known GGA-DFT tendency to underestimate bandgaps). The simulated electronic structure thus yields a robust network of molecular type II heterojunctions in agreement with the experiment.

The behavior of freestanding COF-420 layers was also calculated in order to check that the staggered electronic structure of COF-420 is an intrinsic property and not the result of substrate interactions. The behavior of freestanding COF-420 was found to be nearly identical to COF-420 on Au(111). This can be seen in the projected density of states (PDOS) plots of Figure S3 in the Supporting Information as well as in **Figure 4**a,b which show that the VB and CB wave functions of freestanding COF-420 are separately localized on core A and core B, just as observed experimentally and in the COF-420/Au(111) simulation. The bandgap calculated for freestanding COF-420 is 1.38 eV (Figure S3, Supporting Information), slightly larger than the energy gap calculated for COF-420 on Au(111) (1.10 eV). This difference is expected to be due to the enhanced screening experienced by COF-420 when it is in contact with Au. The band offset obtained from the average energy difference of the VB and VB-1 bands as well as the CB and CB+1 bands for freestanding COF-420 is 0.31 eV, almost identical to the average band offset calculated for COF-420 on Au(111) (0.31 eV), as well as the average experimental offset (0.25 eV).

To understand the microscopic mechanism driving the formation of a periodic array of type II heterojunctions in COF-420, we took a closer look at the simulated charge distribution within the COF network. This suggests that the staggered band structure originates from the dipole field generated by the oriented imine bonds linking the porphyrin cores. The charge distribution was calculated for a freestanding COF-420 single-layer using the Hirshfeld charge analysis as implemented by the Tkatchenko–Scheffler method in the Vienna Ab Initio Simulation Package (VASP) (see Experimental Section). This technique allows evaluation of the difference in charge density that arises in the vicinity of each atom due to the formation of surrounding chemical bonds[5] and has been used to analyze other extended molecular systems.[10] A Hirshfeld population plot of the freestanding COF-420 is shown in Figure 4c. While significant charge redistribution can be seen throughout the COF, the distributed net charge on core A is very similar to the distributed charge on core B (the dashed circles enclose the identical porphyrin macrocycles of core A and core B). The formation of dipoles can be seen between the porphyrin macrocycles that are generated by charge accumulation on the nitrogen atom (blue, $q_N = -0.128$ |e|) as well as the carbon and hydrogen atoms (red, $q_{CH} = 0.075$ |e|) within the imine bonds. The lower energy of core B relative to core A arises because the positive end of the imine dipole always points toward core B, whereas the negative end always points toward core A.

To further test this idea we can perform a rough estimate of the inter-sublattice electrostatic energy offset arising from the dipole field of the oriented imine bonds using the simplified geometry of Figure 4d. For an electron placed at the center of core A, the energy increase arising from the four nearest imine dipoles is

$$\Delta E_A = \frac{1}{4\pi\varepsilon_0} \times \frac{4|e|p}{r^2 - d^2/4} \quad (1)$$

here p is the strength of the imine dipole, d is the length of the dipole, and r is the distance from the dipole center to the core center. The strength of the imine dipole is $p = \frac{q_{CH} - q_N}{2} d$ where q_N is the charge on the nitrogen atom and q_{CH} is the charge on the CH group. From symmetry we see that $\Delta E_B = -\Delta E_A$, and so the energy difference arising from the dipole field for an electron on core A compared to an electron on core B is $\Delta E_T = 2\Delta E_A$. If we use the values $q_N = -0.128$ |e| and $q_{CH} = 0.075$ |e| from the Hirshfeld analysis, $r = 9.53$ Å from the molecular geometry, and $d = 1.29$ Å (the length of a double bond) then we see that $\Delta E_T = 0.16$ eV, in reasonable agreement (given the degree of approximation) with the observed experimental band offset of 0.25 eV.

In conclusion, we have synthesized a porphyrin-based imine-linked square-lattice single-layer COF with atomically-precise type II heterojunctions distributed throughout the entire lattice. Characterization of the COF by STM and spectroscopy measurements and ab initio simulations reveals that an asymmetrical chemical environment of the adjacent porphyrin cores causes localization

© 2018 WILEY-VCH Verlag GmbH & Co. KGaA, Weinheim

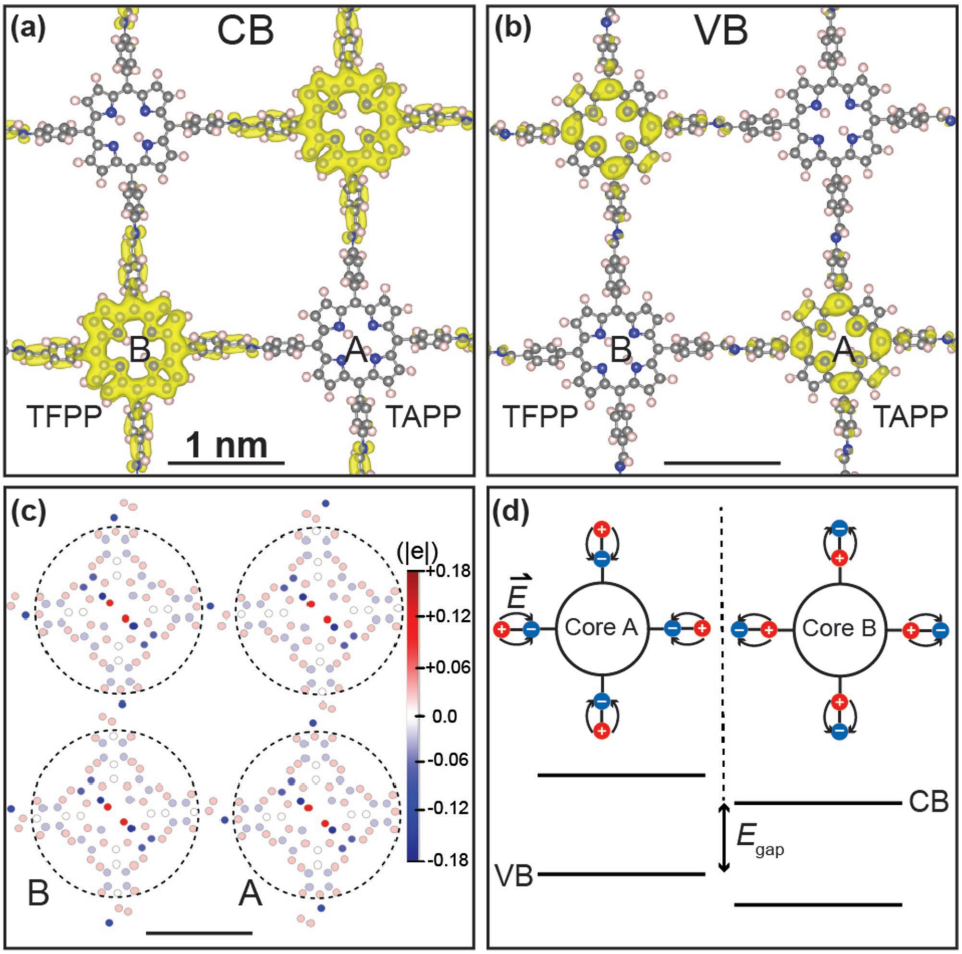

Figure 4. Local charge transfer leads to spatial separation of CB and VB. a) Charge density distribution for free-standing COF-420 state at the CB minimum and b) charge density distribution at the VB maximum. (partial charge density isosurface plotted for 8×10^{-4} |e| $(\text{bohr})^{-3}$). c) Hirshfeld population plot of free-standing COF-420 showing the formation of local dipoles generated by the net charges accumulating on nitrogen atoms (blue, $q_N = -0.128$ |e|), as well as carbon and hydrogen atoms (red, $q_{CH} = 0.075$ |e|) of the imine bonds between porphyrin macrocycles. d) Sketch of a simple electrostatic model showing how the dipole field arising from the oriented imine bonds leads to an energy offset between core A and core B.

of the CB and VB onto distinct COF sublattices. Hirshfeld charge analysis implies that the origin of the heterojunction behavior is the asymmetrical dipole field that arises from oriented imine linkages within the COF. We expect this COF to exhibit novel optoelectronic properties since exciton formation should lead to the generation of electron and hole quasiparticles localized on different COF sublattices.

Experimental Section

Synthesis of meso-Tetra(p-formylphenyl)porphyrin (TFPP): The synthesis of TFPP was carried out according to a literature protocol (Section S4, Supporting Information).[11] In a first step, 4-bromobenzaldehyde was protected using neopentyl glycol to yield 2-(4-bromophenyl)-5,5-dimethyl-1,3-dioxane (90%). In a second step, lithiation at −78 °C followed by formylation with 1-formyl piperidine yielded 4-(5,5-dimethyl-1,3-dioxan-2-yl) benzaldehyde (91%). In a third step, reaction with pyrrole catalyzed by trifluoroacetic acid yielded tetrakis[4-(1,3-dioxa-5,5-dimethylcyclohex-2-yl) phenyl]porphyrin (3%). Finally, deprotection of the 5,5-dimethyl-1,3-dioxane protecting groups yielded meso-Tetra(*p*-formylphenyl)porphyrin which was purified by column chromatography (dichloromethane) and isolated as a dark violet solid (78%).

Surface Growth: Standard Ar^+ sputtering/annealing cycles were applied to a polished Au(111) crystal to yield an atomically clean surface. Molecular precursors for COF-420 were deposited onto the clean Au(111) surface held at room temperature in an UHV environment (base pressure $\approx 2 \times 10^{-10}$ Torr) using a home-built Knudsen-type dual-cell evaporator. The temperature of evaporator for TAPP and TFPP precursors were 330 °C and 340 °C, respectively. The mixed adlayer was then gradually annealed to 180 °C and held at that temperature for 45 min to induce the Schiff-base condensation reaction to form the COF. All STM and STS measurements were performed at $T = 7$K in a home-built cryogenic STM. A Pt/Ir tip was used for all STM measurements. The tip microstructure was changed repeatedly for STM imaging and spectroscopy to rule out tip-based artifacts.

Electronic Structure Calculations: Geometry optimization and electronic structure calculations for freestanding COF monolayers were performed using the projector-augmented wave (PAW) method[12] with the Perdew–Burke–Ernzerhof (PBE) functional[13] (dispersion interactions were taken into account using the Tkatchenko–Scheffler (TS) method[14]). The plane-wave cutoff was set at 400 eV. A Gamma-point-only k-sampling was adopted for geometry optimizations and a $6 \times 6 \times 1$ *k*-mesh generated by the Monkhorst-Pack scheme[15] for the Brillouin zone was used for electronic structure analysis. An energy convergence criterion of 10^{-6} eV was used for

© 2018 WILEY-VCH Verlag GmbH & Co. KGaA, Weinheim

self-consistent calculations while atomic positions were relaxed until the maximal force on each atom was smaller than 0.01 eV Å^{-1}. A 15 Å vacuum layer was placed between periodic images of the COF monolayer to ensure decoupling between neighboring monolayers. Charge transfer values were obtained by the Hirshfeld charge density analysis.[5]

The COF-420/Au(111) system was modeled using a repeated slab approach that included a vacuum region of more than 18 Å along the *z*-direction and four Au layers. The bottom two layers of Au were fixed in their bulk positions (primitive lattice constant = 4.17 Å) while all other atoms in the slab were relaxed to obtain the optimized structure. Dispersion interactions were taken into account using the Tkatchenko–Scheffler vdW^{surf} correction (DFT-vdW^{surf})[16] which has been known to yield accurate absorption heights and binding energies for a variety of atoms and molecules adsorbed on metal surfaces.[16,17] The convergence of the Hellmann–Feynman force was set at 0.02 eV Å^{-1}. To compensate for long-range dipole–dipole interactions among the asymmetric slabs, a dipole sheet was introduced in the middle of the vacuum gap; this procedure leads to zero electric field in the vacuum region, allowing a reliable evaluation of the surface potential.

All quantum-chemical calculations were performed with the VASP.[18]

Supporting Information

Supporting Information is available from the Wiley Online Library or from the author.

Acknowledgements

T.J., C.C., H.L., and C.S.D. contributed equally to this work. This research was supported by the Army Research Office Multidisciplinary University Research Initiative (MURI) program under grant no. W911NF-15-1-0447 (STM spectroscopy), by the Army Research Office grant no. W911NF-17-1-0339 to Georgia Tech (DFT calculations), by the U.S. Department of Energy, Office of Basic Energy Sciences Nanomachine Program under contract no. DEAC02-05CH11231 (COF sample preparation), and by the joint KACST-UC Berkeley Center for Nanomaterials and Clean Energy (molecular synthesis). The KAUST IT Research Computing Team and the KAUST Supercomputing Laboratory are gratefully acknowledged for providing generous computational resources for part of our theoretical work. T.J. acknowledges support from the National Science Foundation (NSF) Graduate Research Fellowship Program under grant no. DGE 1106400. C.S.D. acknowledges support from a Kavli ENSI Philomathia Graduate Student Fellowship. P.J.W. acknowledges the Berkeley Center for Green Chemistry and NSF for support through a Systems Approach to Green Energy Integrative Graduate Education and Research Traineeship (1144885). G.W. acknowledges fellowship support from the National Natural Science Foundation of China under grant no. 61622116, the Strategic Priority Research Program of Chinese Academy of Sciences under grant no. XDB28010200, and the International Partnership Program of Chinese Academy of Sciences under grant no. 112111KYSB20160061.

Conflict of Interest

The authors declare no conflict of interest.

Keywords

covalent organic frameworks, density functional theory, electronic structure, scanning tunneling microscopy and spectroscopy, type II heterojunctions

Received: September 12, 2018
Revised: October 19, 2018
Published online:

[1] a) A. P. Côté, A. I. Benin, N. W. Ockwig, M. O'Keeffe, A. J. Matzger, O. M. Yaghi, *Science* **2005**, *310*, 1166; b) H. M. El-Kaderi, J. R. Hunt, J. L. Mendoza-Cortés, A. P. Côté, R. E. Taylor, M. O'Keeffe, O. M. Yaghi, *Science* **2007**, *316*, 268; c) C. S. Diercks, O. M. Yaghi, *Science* **2017**, *355*, eaal1585.

[2] a) C. S. Diercks, S. Lin, N. Kornienko, E. A. Kapustin, E. M. Nichols, C. Zhu, Y. Zhao, C. J. Chang, O. M. Yaghi, *J. Am. Chem. Soc.* **2018**, *140*, 1116; b) C. R. DeBlase, K. Hernández-Burgos, K. E. Silberstein, G. G. Rodríguez-Calero, R. P. Bisbey, H. D. Abruña, W. R. Dichtel, *ACS Nano* **2015**, *9*, 3178; c) S. Wan, J. Guo, J. Kim, H. Ihee, D. Jiang, *Angew. Chem., Int. Ed.* **2009**, *48*, 5439; *Angew. Chem.* **2009**, *30*, 5547; d) S. Wan, J. Guo, J. Kim, H. Ihee, D. Jiang, *Angew. Chem., Int. Ed.* **2008**, *47*, 8826; *Angew. Chem.* **2008**, *46*, 8958.

[3] a) M. S. Lohse, T. Bein, *Adv. Funct. Mater.* **2018**, *28*, 1705553; b) S. Y. Ding, W. Wang, *Chem. Soc. Rev.* **2013**, *42*, 548.

[4] a) X. Feng, L. Chen, Y. Honsho, O. Saengsawang, L. Liu, L. Wang, A. Saeki, S. Irle, Y. Dong, D. Jiang, *Adv. Mater.* **2012**, *24*, 3026; b) S. Jin, X. Ding, X. Feng, M. Supur, K. Furukawa, S. Takahashi, M. Addicoat, M. E. El-Khouly, T. Nakamura, S. Irle, S. Fukuzumi, A. Nagai, D. Jiang, *Angew. Chem., Int. Ed.* **2013**, *52*, 2017; *Angew. Chem.* **2013**, *125*, 2071; c) S. Jin, K. Furukawa, M. Addicoat, L. Chen, S. Takahashi, S. Irle, T. Nakamura, D. Jiang, *Chem. Sci.* **2013**, *4*, 4505; d) G. H. V. Bertrand, V. K. Michaelis, T.-C. Ong, R. G. Griffin, M. Dincă, *Proc. Natl. Acad. Sci. USA* **2013**, *110*, 4923; e) M. Dogru, M. Handloser, F. Auras, T. Kunz, D. Medina, A. Hartschuh, P. Knochel, T. Bein, *Angew. Chem., Int. Ed.* **2013**, *52*, 2920; *Angew. Chem.* **2013**, *125*, 2992.

[5] F. L. Hirshfeld, *Theor. Chim. Acta* **1977**, *44*, 129.

[6] W. Auwarter, A. Weber-Bargioni, S. Brink, A. Riemann, A. Schiffrin, M. Rubin, J. V. Barth, *ChemPhysChem* **2007**, *8*, 250.

[7] W. Chen, V. Madhavan, T. Jamneala, M. F. Crommie, *Phys. Rev. Lett.* **1998**, *80*, 1469.

[8] a) T. Yokoyama, S. Yokoyama, T. Kamikado, S. Mashiko, *J. Chem. Phys.* **2001**, *115*, 3814; b) W. Auwärter, K. Seufert, F. Klappenberger, J. Reichert, A. Weber-Bargioni, A. Verdini, D. Cvetko, M. Dell'Angela, L. Floreano, A. Cossaro, G. Bavdek, A. Morgante, A. P. Seitsonen, J. V. Barth, *Phys. Rev. B* **2010**, *81*, 245403; c) Q. Zhang, X. Zheng, G. Kuang, W. Wang, L. Zhu, R. Pang, X. Shi, X. Shang, X. Huang, P. N. Liu, N. Lin, *J. Phys. Chem. Lett.* **2017**, *8*, 1241; d) C. Chen, T. Joshi, H. Li, A. D. Chavez, Z. Pedramrazi, P.-N. Liu, H. Li, W. R. Dichtel, J.-L. Bredas, M. F. Crommie, *ACS Nano* **2018**, *12*, 385.

[9] a) M. S. Hybertsen, S. G. Louie, *Phys. Rev. B* **1986**, *34*, 5390; b) J. B. Neaton, M. S. Hybertsen, S. G. Louie, *Phys. Rev. Lett.* **2006**, *97*, 216405.

[10] E. Carbonell-Sanromà, J. Hieulle, M. Vilas-Varela, P. Brandimarte, M. Iraola, A. Barragán, J. Li, M. Abadia, M. Corso, D. Sánchez-Portal, D. Peña, *ACS Nano* **2017**, *11*, 7355.

[11] S. Hong, M. R. Rohmann, J. Jia, Y. Kim, D. Moon, Y. Kim, Y. H. Ko, E. Lee, K. Kim, *Angew. Chem., Int. Ed.* **2015**, *54*, 13241; *Angew. Chem.* **2015**, *45*, 13439.

[12] P. E. Blöchl, *Phys. Rev. B* **1994**, *50*, 17953.

[13] J. P. Perdew, K. Burke, M. Ernzerhof, *Phys. Rev. Lett.* **1996**, *77*, 3865.

[14] A. Tkatchenko, M. Scheffler, *Phys. Rev. Lett.* **2009**, *102*, 73005.

[15] H. J. Monkhorst, J. D. Pack, *Phys. Rev. B* **1976**, *13*, 5188.

[16] V. G. Ruiz, W. Liu, E. Zojer, M. Scheffler, A. Tkatchenko, *Phys. Rev. Lett.* **2012**, *108*, 146103.

[17] a) W. Liu, J. Carrasco, B. Santra, A. Michaelides, M. Scheffler, A. Tkatchenko, *Phys. Rev. B* **2012**, *86*, 245405; b) W. A. Al-Saidi, H. Feng, K. A. Fichthorn, *Nano Lett.* **2012**, *12*, 997; c) C. Wagner, N. Fournier, F. S. Tautz, R. Temirov, *Phys. Rev. Lett.* **2012**, *109*, 76102; d) W. Liu, S. N. Filimonov, J. Carrasco, A. Tkatchenko, *Nat. Commun.* **2013**, *4*, 2569.

[18] a) G. Kresse, J. Furthmüller, *Comput. Mater. Sci.* **1996**, *6*, 15; b) G. Kresse, J. Furthmüller, *Phys. Rev. B* **1996**, *54*, 11169.

© 2018 WILEY-VCH Verlag GmbH & Co. KGaA, Weinheim